Combining suction and friction to stabilize a soft gripper to shear and normal forces, for manipulation of soft objects in wet environments

Jessica A. Sandoval[1], Thomas Xu[2], Iman Adibnazari[1], Dimitri D. Deheyn[2], Michael T. Tolley[1]

Abstract—Soft robotic gripping in wet environments is generally limited by the presence of a liquid that lubricates the interface between the gripper and an object being manipulated. The use of soft grippers is particularly beneficial for manipulating soft, delicate objects, yet is further limited by low grip strengths. We propose the use of suction, a form of adhesion that functions well in wet environments, to enhance soft robotic grippers. We stabilized the suction against shear disturbances using soft actuated fingers decorated with fluid-channeling patterns to enhance friction, counteracting the interfacial lubrication experienced in wet environments. We therefore combined the uses of attachment via suction and shear stability via friction to create an adhesive soft gripper. We evaluated the contributions to attachment of each component to help stabilize it against dislodgement forces that act in parallel and normal to an object that it aimed to manipulate. By identifying these contributions, we envision that such an adhesive gripper can be used to benefit soft robotic manipulation in a variety of wet environments, from surgical to subsea applications.

Index Terms—Soft Robot Materials and Design, Grippers and Other End-Effectors

I. INTRODUCTION

A Wet environment poses a challenge for soft robotic gripping. The presence of water, or any other fluid, acts to lubricate a surface, thus reducing the friction needed to achieve a stable grasp [1], [2]. Soft grippers, like human hands, exert a force on an object, perpendicular to the surface in an effort to maintain its grasp [3]. This force is related to the amount of friction between the gripper and the object being manipulated [4]. For grippers with high coefficients of friction, the force required to maintain a stable grasp is reduced, allowing for more delicate manipulation [4]. Additionally, the use of elastomers in soft robotic grippers further enhances the ability to delicately manipulate a surface while minimizing the potential for damage [5].

A pneumatic soft gripper is composed of a series of internal chambers, that upon inflation, results in a bending motion. When grasping objects, soft grippers face the challenge of generating sufficient grip forces to support a payload [5]. The design of the pneumatic channels have been tailored to improve load distribution [6], yet the generated force is still low compared to the forces generated by manipulators composed of rigid components. To yield a higher load capacity, adhesives, such as gecko-inspired adhesives, have been applied to soft grippers [6]. However, in the presence of water, dry adhesives are rendered ineffective [7]. Thus, alternative adhesive strategies that function within a wet environment must be used to enhance gripping in the case of interfacial lubrication.

One adhesive mechanism that works well in a wet environment is suction, which generates high adhesive forces normal to a surface, thus supporting the grip of a wetted object. Previous work has demonstrated that the use of suction at the end of robotic fingertips helps to increase the coefficient of friction and normal force of the robotic hand against wetted objects [8]. Suction has shown promise for its ability to grasp delicate, irregular, and even rough surfaces [9]. However, dependent on the design of the suction device, some designs have reported low coefficients of friction when used on wetted surfaces [10]. Enforcing the shear stability of a suction-based gripper would be crucial for preventing slippage along a wet surface.

Surface texturing has been demonstrated to improve coefficients of friction against wet objects. The use of textures and surface structures to successfully grip in wet environments is not unique to robotic systems, however. Organisms ranging from insects to fish use a variety of surface structures and textures to help stabilize their grip to wet surfaces [11]. The surface structures vary in type. For instance, organisms such as beetles use arrays of microstructured setae, which are mediated by either secretions or modified suckers, to successfully attach in wet conditions [12]. Whereas organisms, such as the tree frog [13], bush cricket [14], and clingfish [15], all exhibit

Manuscript received October 11, 2021; Revised January 12, 2022; Accepted January 24, 2022.

This paper was recommended for publication by Editor Kyu-Jin Cho upon evaluation of the Associate Editor and Reviewers' comments. This work was supported by the Office of Naval Research grant number N000141712062. J. Sandoval is supported by the Gates Millennium Scholars (GMS) program.

[1]Jessica Sandoval, Iman Adibnazari, and Michael T. Tolley are with the Department of Mechanical and Aerospace Engineering, University of California San Diego, 9500 Gilman Dr., La Jolla, CA 92093, USA. jas164@eng.ucsd.edu

[2]Thomas Xu is with the Department of Mechanical Engineering, Carnegie Mellon University, 5000 Forbes Ave, Pittsburgh, PA 15213, USA.

[3]Dimitri Deheyn is with the Marine Biology Research Division, Scripps Institution of Oceanography, 9500 Gilman Dr., La Jolla, CA 92093, USA.

Digital Object Identifier (DOI): see top of this page.

hexagonal surface texturing to engage with wet surfaces.

These organisms have inspired the development of biomimetic surface structures and textures to attach in wet environments. For instance, the beetle inspired the development of arrays of high aspect ratio, mushroom-shaped microstructures [16], some of which exhibit concavities to enable suction [17], to successfully attach underwater. Conversely, the tree frog, bush-cricket, and clingfish helped to inspire the development of hexagonal frictional textures [14], [15], [18] that function based on the principles of wet adhesion and friction [19]. For this paper, we focus on the contributions of bioinspired hexagonal surface textures to attachment in underwater domains.

The bioinspired hexagonal surface textures function to shuttle fluid from beneath the area of contact into channels between the textures, resulting in greater contact and an improved coefficient of friction [18], [20]. Overall, these bioinspired textures have been demonstrated to improve the resistance to shear forces that act parallel to a surface.

In this work, we coordinated the advances of surface textures, suction, and soft actuation to develop an adhesive gripper that is capable of attaching to wet surfaces. We investigated the relative contributions of each of these three components to successful attachment against disturbances that act parallel, or along the x-direction of the coordinate frame, and normal, along the z-direction, to a surface. Additionally, to narrow the scope of this study, we only considered gripping large objects that were too wide to envelop in an enclosing grasp.

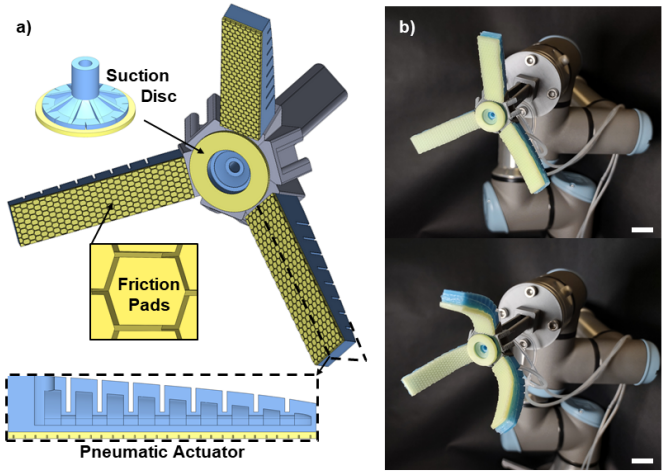

Fig. 1. Overview of the adhesive gripper. a) Schematic of the adhesive gripper. A central suction disc is flanked by three fingers composed of fluidic elastomer actuators (FEAs), which bend to engage a frictional texture with the surface of a target object. The actuators have internal pneumatic chambers with parabolically decreasing internal geometry to achieve even surface conformation. b) Photographs of unactuated (top) and actuated (10 psi, bottom) states of the pneumatic fingers. The gripper is mounted to a commercial robotic arm. Scale bar, 20 mm.

II. RESULTS

A. Design of an adhesive gripper

The adhesive gripper was designed to provide a stable, delicate grip by combining suction, friction, and soft actuation. The gripper was composed of three components: 1) a suction disc to provide strong adhesion normal to the surface, 2) friction pads to provide resistance to shear forces along the x-direction, and 3) fluidic elastomer actuators (FEAs) to engage the friction pads with the surface of a target object (Fig. 1). In this work, the FEAs combined with the friction pads are referred to as a unit as textured fingers.

At the center of the gripper, a suction disc, composed of soft elastomers consistent with our previous work [9] served to provide strong axial adhesion to wet surfaces. To stabilize against shear forces of dislodgement, three fingers composed of friction pads were equidistantly spaced around the central axis of the gripper. The friction pads consisted of a textured surface composed of elongated hexagons (aspect ratio: 1.3), which we found in previous work to increase the coefficient of friction when subjected to shear loads [15]. The hexagons were designed with a width, length, and height of 1.3, 2.1, and 1.0 mm, respectively.

We used soft actuators containing a network of pneumatic chambers [21] to bend upon inflation to engage the friction pads with a surface. We used an inextensible strain-limiting layer along the length of the actuator to enforce a bending behavior.

B. Simulation of surface conformation of the textured fingers

We aimed to engage as much of the friction pads as possible with the target surface. A greater amount of friction pads in contact with the surface would allow for a higher occurrence of fluid channeling, thus allowing for more intimate contact to be achieved with the surface [22]. Additionally, by increasing the amount of contact that the gripper made with a surface, we would reduce the compressive load on the object and distribute it over a larger surface area, thus enabling a more delicate grip. Thus, a uniform surface conformation was critical. Using simulation, we tested the difference in contact between two geometries of the pneumatic chambers. We chose to investigate a rectangular and a parabolic geometry of the pneumatic chambers. The selection of a parabolic pneumatic chamber was based on previous work which found that this geometry resulted in a non-uniform bending moment along the length of the actuator [6].

Additionally, we simulated how the different geometries interacted with a cylindrical surface that varied in stiffness from soft to stiff (0.005, 0.05, and 0.5 MPa) to rigid (50 GPa) (Fig. 2 a). Please refer to the Materials and Methods section for further details of the setup of the simulation.

Across the four tested surface stiffnesses, we monitored the percentage of the actuator in contact with the surface of the cylinder (Fig. 3). The actuator with a parabolic

internal geometry maintained consistently at least double the amount of contact with the simulated surface in comparison to the actuator with a rectangular internal geometry (Fig. 2 c). The actuator with parabolic chambers demonstrated greater surface contact with surfaces of a stiffness greater than 0.05 MPa (i.e. 83% and 79% for 0.05 and 0.5 MPa, respectively) in comparison with the softest of the surfaces (61%; 0.005 MPa). The actuator of a rectangular internal geometry maintained a significantly lower percentage of contact, at an average of 28%, with the simulated surface. The surface contact of the actuator with a rectangular internal geometry did not vary across the surface stiffnesses, where the softest and stiffest of surfaces tested exhibited a consistent, although low, area of contact.

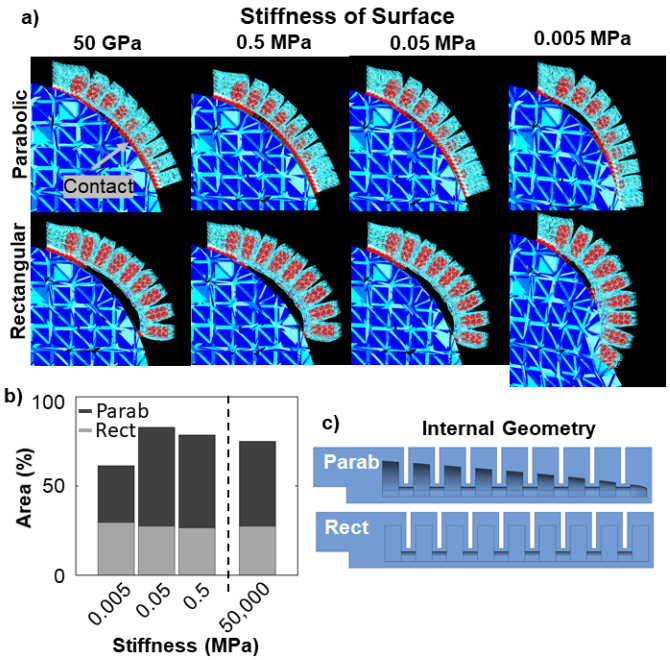

Fig. 2. Simulation of the contact made by an actuator against a cylindrical surface. a) Simulation of the contact made by an actuator of either parabolic (top row) or rectangular (bottom row) internal geometries, against a cylindrical object that varied in stiffness (left to right, 50 GPa, 0.5 MPa, 0.05 MPa, and 0.005 MPa). b) We measured the percentage of the total surface area of the soft finger that was in contact with the simulated surface upon actuation. We compared the contact area of the soft finger with parabolic (dark gray) and rectangular (light gray) internal geometries. c) Cross-sectional view of the pneumatic chambers of the actuator.

The actuators of parabolic and rectangular pneumatic chambers differed in the distribution of contact and overall bending behavior. The parabolic internal geometry resulted in a greater distribution of contact, most specifically extending from the middle to the tip of the actuator (Fig. 3). The bending behavior of the actuator with a parabolic pneumatic chamber therefore demonstrated a higher degree of surface conformation (Fig. 2 a). The rectangular internal geometry resulted in a lower distribution of contact, which was instead concentrated at the base and tip of the actuator (Fig. 3). As the actuator of a rectangular pneumatic chamber contacted the surface,

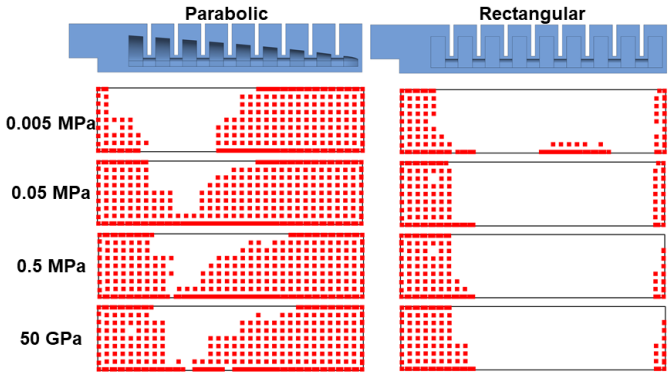

Fig. 3. Map of surface contact, as quantified in simulation. a) A visual representation of the nodes in contact with the cylindrical surface upon actuation of the actuators with parabolic (left) and rectangular (right) internal geometries. We varied the stiffness of the surface from soft (0.005 MPa; top row) to rigid (50 GPa; bottom row).

the middle of its length buckled and bent away from the surface, leading to the concentration of contact in only its base and tip (Fig. 2 a). This buckling led to an apparent pinching behavior of the actuator and an overall loss of surface contact.

From the visualization of surface contact, we observed that the simulated behavior demonstrated some asymmetries. The body of the actuator would twist slightly, causing an asymmetric behavior. The twist was attributed to minor differences in the meshes of the body of the actuator and the internal air chambers, and to surface interactions with the highly deformable cylindrical surface.

Thus, we concluded that since the pneumatic chambers with parabolically decreasing internal area was most successful at engaging with the surface of a soft target object in simulation, we chose this design for our experimental investigations.

C. Resistance to shear forces in a wet environment

We tested the contributions of the components of the gripper to resisting shear disturbances (Fig. 4). To perform this characterization, we secured the gripper as an end effector to a robotic arm, which was used to record the forces from manipulation. We translated the gripper a distance of 30 mm in the x-direction, along a plane tangent to the top of a hemispherical surface, which was submerged in a bath of water (Fig. 4 a). We varied the stiffness of the hemispherical surface to quantify the effect of surface stiffness on the resistance to shear disturbances.

To elucidate the contribution of suction and friction to the magnitude of the aforementioned resistance to shear disturbances, we ran experiments with the gripper in one of four configurations–all components (suction and textured fingers) active (S.T.), only suction active (S. only), only the textured fingers active (T. only), or a control, in which all components were inactive (Ctrl.) (Fig. 4 b). Unless otherwise indicated, the textured fingers in an active configuration were actuated by 10 psi of air

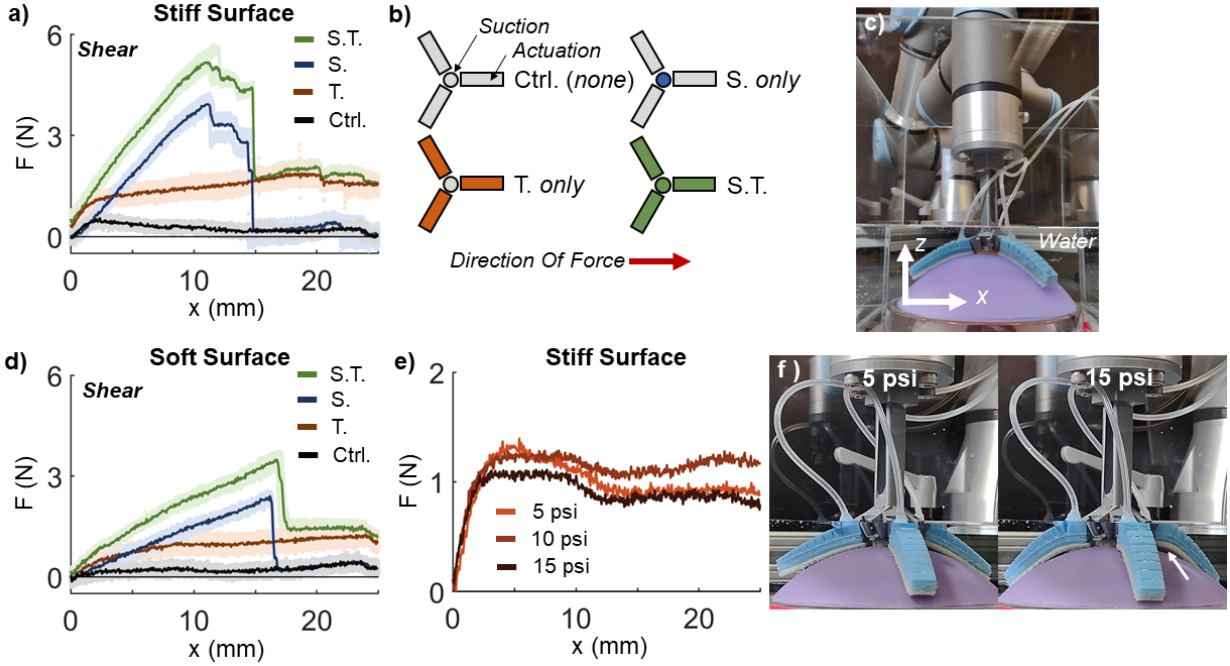

Fig. 4. Contribution of suction and friction to shear stability to soft surfaces. a) Force measurements quantifying the contribution of suction and friction to resisting shear motions, while engaged with a stiff surface. The gripper was sheared for a total of 30 mm in the x-direction. The averaged, interpolated force-extension curve is shown as a dark line. The shaded region represents the standard deviation across three trials. Color coordination corresponds to subfigure b. b) The control (dark gray), in which neither the suction or actuation of the soft fingers were active. The suction only (S. only; blue) configuration, in which only the central suction chamber was active. The textured fingers only (T. only; orange) configuration, in which only the frictional actuators were active. The suction and soft fingers (S.T.; green) configuration, in which both the suction disc and the textured fingers were active. c) Experimental setup of force measurements. The gripper was attached as an end effector to a robotic arm. All tests took place in a bath of water, water line indicated in white. d) Force measurement quantifying resistance to shear (x-direction) motions of a gripper, against a soft surface. e) Quantification of actuation pressure of the pneumatic gripper. We tested the actuation pressures of 5 (light orange), 10, and 15 (darkest orange) psi. The test was performed on a stiff surface ($E_{surface}$, 0.165 MPa) . f) Gripper engaged with the surface with either 5 (left) or 15 (right) psi. The use of 15 psi to actuate the gripper caused disengagement with the surface (arrow).

pressure. Prior to the trial, the suction disc was preloaded to the surface by imparting a displacement on the back of 1 mm. For the reported adhesive forces per configuration type, we linearly interpolated the raw data per trial to generate a trendline for the force-displacement curve that accounted for noise. We then averaged the interpolated adhesive curves, which are reported in (Fig. 4 c). We found that, when gripping a stiff elastomeric surface, the use of both suction and textured fingers resulted in the highest shear force (S.T.; 5.3 $\pm$ 0.3 N; Fig. 4 c), which was 1.3 times greater than the use of suction alone (S; 3.96 $\pm$ 0.16 N) and 2.75 greater than the use of the textured fingers alone (F; 1.92 $\pm$ 0.17 N). The combined suction and textured fingers had a shear force that was 8.9 times greater than the control (0.59 $\pm$ 0.06 N). These results demonstrated that the effects of suction and actuated, textured fingers were linearly additive to the resulting shear force.

When comparing the resistance to shear motions between surface types, we found that using a soft surface ($E_{surface}$, 0.0065 MPa) that was about two orders of magnitude less stiff in comparison to the stiff ($E_{surface}$, 0.165 MPa) elastomeric surface resulted in a 32% reduction in shear force for the S.T. (3.6 $\pm$ 0.2 N) and T. (1.3 $\pm$ 0.2 N) configurations and a 39% reduction for the S. (2.4 $\pm$ 0.1 N) configuration. The force curves exhibited different behaviors, where the soft surface corresponded to sharp transitions in the force-displacement curves. The shear force for the stiff surface, by comparison, demonstrated a step-wise transition from the maximum force to a sharp vertical transition. This more gradual transition was attributed to an apparent stick-slip behavior of the suction disc as it was sheared, resulting in a buckling in the suction chamber while still attached, likely causing a temporary leak in its seal and thus lower adhesive force.

We quantified the effect of the pressurization of the pneumatic chambers to select the ideal operating pressures for the experiments. We found that while low pressures of the pneumatic chambers still served to adequately engage the frictional textures to the surface, over-pressurizing would result in a reduction of shear force. Pressurization of the textured fingers with 5 and 10 psi resulted in a consistent shear force of 1.4 $\pm$ 0.1 N across the two pressures. Pressurization to 15 psi resulted in a drop in shear force to 1.2 $\pm$ 0.2 N. Visually, we observed a buckling of the actuator from the surface at 15 psi that was not observed at 5 psi (Fig. 4 f).

To understand the variability in the shear force as a function of the rotation of the three-fingered gripper around its central axis, we quantified the effect of the

orientation of the gripper on its shear force. The gripper was considered to be either in a "forward" orientation, when the gripper moved in a direction toward one of the fingers, or in a "trailing" orientation, when the gripper moved in a direction away from one of the fingers (see Fig. 5c).

We found that the orientation affected the shear force more when gripping a stiff rather than soft surface. That is, a change in the orientation from Forward to Trailing on the stiff surface resulted in a 12% reduction in shear force for the suction and friction (S.T.) configuration, and a 27% reduction in performance for the textured finger (T.) configuration (Fig. 5 a).

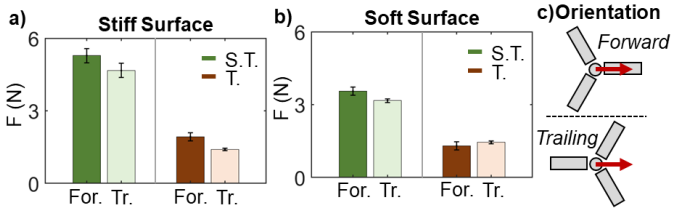

Fig. 5. Effect of orientation of the gripper on shear adhesion. a) The difference in adhesive force of a gripper in the forward (For., dark shade) and trailing (Tr., light shade) orientations for the S.T. and T. configurations when tested against a stiff surface. b) The difference in adhesive force, dependent on orientation, when tested against a soft surface. Error bars indicate one standard deviation; all trials were performed in triplicate. c) Schematic of the orientations of the gripper.

Conversely, for the soft surface, the effect of the orientation was less apparent. The suction and textured finger orientation (S.T.) resulted in a 10% reduction in shear force by changing from forward to trailing configurations. Conversely, the configuration of only actuated textured fingers (T.) resulted in an 11% increase in shear force (Fig. 5 b).

D. Normal adhesion in a wet environment

We tested the contributions of the components of the gripper at resisting dislodgement normal to the testing surface. We retracted the arm in the z-direction at a constant rate for a total of 15 mm. Against a stiff elastomeric testing surface, the adhesive gripper generated higher normal forces than against a soft surface. The combination of active suction and textured fingers (S.T.) resulted in an adhesive force of 4.9 ± 0.2 N, followed by the suction only (S.) configuration, with an adhesive force of 3.6 ± 0.2 N. The actuated textured fingers alone (T.) resulted in a normal force of 2.2 ± 0.2 N. We observed a difference in normal force responses, dependent on the type of actuation involved. The suction disc resulted in a sharp vertical transition from the absolute maxima to 0 N. Conversely, the textured fingers alone resulted in a constant force which plateaued across the force-displacement curve. We attributed this plateau to the fact that a displacement of 15 mm in the z-direction was still less than the length of the finger, and thus while the fingers

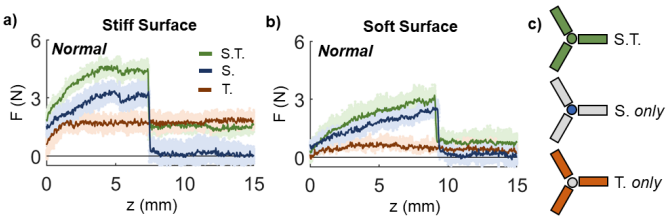

Fig. 6. Contribution of suction and friction to adhesion of the gripper normal to the surface. a) Force of axial adhesion resulting from 15 mm displacement in the z-direction, against a stiff hemispherical surface in water. The data was linearly interpolated and averaged across three trials. The raw data from the three trials is indicated by the light shading. The averaged interpolated curve is indicated by the dark line, corresponding to the color of the configuration. Suction and textured fingers actuated (S.T.; green). Suction only activated (S.; blue). Textured fingers only actuated (T.; orange). b) Axial adhesion of gripper against a soft, hemispherical surface in water. c) Configuration of the gripper, the color of which corresponds to the plots.

were still in contact with the surface, the resulting force would be predominantly due to friction.

Comparing the performance of the components, we investigated the effect of a soft surface on the resulting normal force. We found that the use of the gripper against a soft surface resulted in a reduction of adhesive force across all components tested, most significantly for the actuated textured fingers. For only the actuated fingers, changing from a stiff to a soft surface resulted in a 56% reduction in normal force (T. at soft surface; 1.0 ± 0.3 N). Suction was less affected by the change in surface stiffness, in comparison to the textured fingers, with a 23% reduction in normal force for suction alone (S. on soft surface; 2.8 ± 0.2 N). The configuration of active suction and textured fingers resulted in a 32% reduction of adhesive force (S.T.; 3.3 ± 0.3 N).

E. Application of the adhesive gripper

The adhesive gripper was able to manipulate a variety of objects, ranging in stiffness and surface roughness. For these trials, we mounted the gripper as an end effector to a robotic arm to accomplish a variety of tasks. We used the gripper to manipulate a pumpkin while submerged in a bath of water (Fig. 7, Mov. S1). Weights were added to the pumpkin to result in negative buoyancy. The robotic arm was used to subject the gripper to a range of forces and motions, including a combination of shear, rotational, and normal forces. We varied the vertical velocity of the movements of the arm from 20 mm/s to a maximum of 100 mm/s. Across the trials, the adhesive gripper maintained a stable grip of the pumpkin, even at high velocities.

In addition, we demonstrated the use of the gripper at grasping a variety of surface roughnesses. For instance, the gripper successfully grabbed a ceramic vessel, which exhibited a rough surface texture, while submerged in a bath of water (Fig. 8 a). Overall, the gripper was able to support a maximum load normal to the object of 500 g (4.9 N) in submerged conditions.

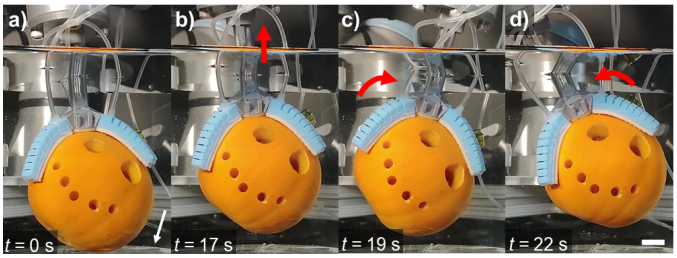

Fig. 7. Demonstration of underwater manipulation using a robotic arm. a) The adhesive gripper successfully grasped a pumpkin submerged in a bath of water (t = 1 s). b) The gripper lifted the pumpkin off the testing surface (t = 17 s). c) The gripper rotated the pumpkin clockwise by 20° (t = 19 s). d) The gripper rotated the pumpkin counterclockwise by 50° (t = 22 s). Scale bar, 20 mm.

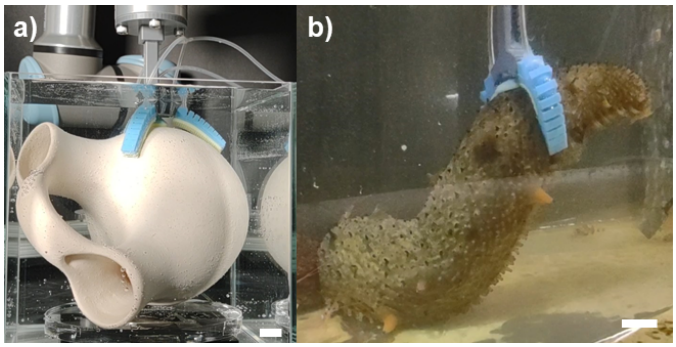

Fig. 8. Versatile applications of the adhesive gripper. a) A successful grasp onto the rough surface of a ceramic vessel. b) Manipulation of a live sea cucumber. Both trials occurred in a submerged environment. Scale bars, 20 mm.

We also demonstrated the ability of the adhesive gripper to handle delicate biological specimen (Fig. 8 b). The gripper was able to delicately attach on to, grip, and manipulate a live sea cucumber. The sea cucumber has a very soft and deformable body with considerable, raised texturing along the epidermis. The gripper did not need to fully envelop the sea cucumber for a successful grasp, as the combination of suction and gentle pressure exerted by the textured fingers was enough to maintain a stable yet gentle grasp without harm to the organism.

III. Discussion

In this work, we evaluated the contribution of suction and friction to resist disturbances of forces that acted shear and normal to large, hemispherical surfaces. We performed these trials on large objects, such that the gripper was unable to achieve an enclosing grasp. By evaluating the effects of these components to the stability of a soft robotic gripper, we can aid in successful gripping of large, soft objects in wet environments.

We found that the each component (suction, friction) was linearly additive to the resulting force that acted to resist disturbances. That is, the frictional, textured fingers supplemented the adhesive strength of suction. This finding suggests that combining suction and frictional textures can benefit the stability of the grasp of a soft robotic gripper, thus enabling soft manipulators with a strong, yet delicate, grasp.

The use of adhesion, friction, and soft actuation benefits the objective of manipulation in wet and submerged environments while maintaining a delicate touch. This is especially important in the areas of surgical and subsea robotics. For surgical manipulations, the delicate organ tissue can easily be damaged by rigid manipulators, which are orders of magnitude stiffer than the tissue that they aim to manipulate [23]. While frictional textures have been previously demonstrated on surgical manipulators [18], our results suggest that coupling adhesion via suction would enhance the strength of the grip without the need to exert high compressive loads on the tissue.

We anticipate that the coupling of suction and friction would also be beneficial to the field of subsea robotic manipulations, in which a gentle touch is vital for the recovery of archaeological and biological specimen. In this paper, we have demonstrated a few preliminary use cases by handling ceramic vessels, as a proxy for archaeological artifacts, and very soft, deformable marine organisms, such as sea cucumbers. We suggest that further exploration into coupling suction and friction via texturing can further enable delicate manipulation in underwater robotics.

IV. Materials and Methods

A. Fabrication of the adhesive gripper

The adhesive gripper was composed of a suction chamber and pneumatic actuators, which were fabricated separately and combined using a modular support collar. All components of the gripper were modeled using computer-aided design (Solidworks, Dassault Systems). The support collar for the gripper was fabricated from PLA using a 3D printer (Prusa i3 MK3S+). The support collar angled the base of the actuators by 60° relative to the central axis of the suction disc. The pneumaic actuators were designed with a length of 46 mm, width of 11 mm, and height of 10 mm. The pneumatic actuator was produced using a custom mold that was made of a hard resin (VeroClear, Stratasys Inc.) on a multimaterial 3D printer (Object 350 Connex3, Stratasys, Inc.). After printing, the mold for the pneumatic actuator was aged for 4 h at 40°C to ensure that the resin had fully cured. The actuators were molded using silicone rubber (stiffness, 0.231 MPa; Dragon Skin 20, Smooth-On, Inc.). Uncured silicone was added to the mold for the pneumatic network, degassed for 5 min, and cured for 4 hr (Fig. 9). Uncured silicone was added to the mold for the strain-limiting layer and degassed for 2 min. A strip of paper was embedded in the silicone to serve as the inextensible layer. After fully curing, the elastomeric body was bonded to the strain-limiting layer using a silicone adhesive (Sil-Poxy, Smooth-On, Inc.).

We fabricated the frictional textures using soft silicone rubber (Young's modulus, 0.0167 MPa; Ecoflex 00-20, Smooth-On Inc.). The mold (Fig. 9 c) for the texture was etched into acrylic using a laser machining system (PLS6MW, Universal Laser Systems). The texture was

This article has been accepted for publication in a future issue of this journal, but has not been fully edited. Content may change prior to final publication. Citation information: DOI 10.1109/LRA.2022.3149306, IEEE Robotics and Automation Letters

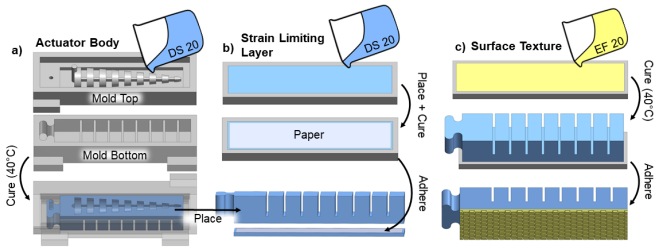

Fig. 9. Fabrication steps of the textured fingers. a) The body of the actuator was molded with a stiff elastomer (Dragon Skin 20; blue). b) The strain limiting layer was molded separately. A strip of paper served as the strain-limiting element of the layer. The body of the actuator and the strain limiting layer were adhered together using silicone adhesive. c) The surface texture was molded using a soft elastomer. The fully cured texture was applied to the bottom of the actuator using silicone adhesive. This completed assembly is referred to as a textured finger.

composed of an array of elongated hexagons [15] with a width, length, and height of approximately 1.6 mm, 2.1 mm, and 1.0 mm, respectively. Uncured silicone was added to the mold, degassed for 5 min, and cured for 6 h. The frictional texture was then bonded to the strain-limiting layer using silicone adhesive.

We fabricated the suction discs using a 3D printed mold for the suction chamber. Uncured silicone (Dragon Skin 20, Smooth-On, Inc.) was added to the mold of the suction chamber, degassed for 5 min, and cured at 40°C. A soft sealing layer (Ecoflex 00-20, Smooth-On Inc.) was added to the disc margin of the suction chamber. The uncured silicone was first added to a mold, partially cured at 40°C for 5 minutes, and bonded to the suction chamber using uncured silicone. These two components were allowed to cure together at 40°C for 1 hr.

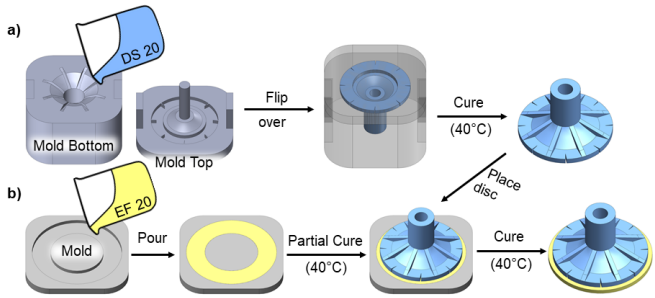

Fig. 10. Fabrication steps of the suction disc. a) The suction chamber was molded from a stiff elastomer (DragonSkin 20; blue) and cured in the mold at 40°C. b) The sealing layer of the suction disc was molded using a soft elastomer (Ecoflex 00-20; yellow), and partially cured at 40°C. The fully cured suction chamber was applied to the back of the sealing layer, and subsequently fully cured together.

B. Simulation of the contact made by an actuator

We simulated the contact of the actuator with a surface using an open-source physics simulation software (Simulation Open Framework Architecture, SOFA, v20.06). We first modeled using CAD (SolidWorks, Dassault Systems) the actuator and the test object. The test object was a cylindrical object (radius, 13 mm), for which we varied the stiffness across the trials from 0.005, 0.05, and 0.5 MPa and 50 GPa. From the CAD models, we generated the surface meshes of the objects which were used in SOFA for collision detection. We also generated volumetric meshes to model internal forces and object deformation, using an open-source mesh generation software (Gmsh v4.5.6).

The simulation was set up using an implicit, first-order numerical integration scheme (module, "EulerImplicitSolver"), and was solved at each time step using LDL decomposition (module, "SparseLDLSolver"). Compliance matrices were also solved directly at each time step (module, "LinearSolverConstraintCorrection"). The simulated actuator was pressurized by applying pressure to the surface elements of the mesh of the pneumatic cavity (module, "SurfacePressureConstraint"). We then used a Barycentric mapping component to couple the motions of the cavity mesh and body mesh.

In the simulated environment, we assumed that the actuator and test object had diagonal mass matrices, Poisson ratios of 0.3, and a mutual coefficient of friction of 0.3. We assumed that their materials were linear and isotropic, providing the same resistance to strain in all directions.

The elastic modulus of the body of the actuator was 3.4 MPa, consistent with silicone elastomers. Additionally, the strain-limiting layer in the body of the actuator was modelled as a layer that was 2 mm thick of a high elastic modulus (50 GPa).

Each test performed in the simulation was conducted in the absence of gravity, with a time step of 0.02 s, and with an average test duration of 7.5 s. The pressure within the pneumatic cavity was increased linearly at a rate of 0.001 MPa per 0.06 s, up to a maximum pressure of 0.06 MPa. The body of the actuator was angled 15° from horizontal and was offset from the centerline of the test object. The base of the actuator, as well as $\frac{3}{4}$ of the cylindrical object, were fixed in space during tests. We monitored the area of the actuator in contact with the test surface upon inflation.

C. Force measurements using a robotic arm

We measured the force of the gripper to a submerged, hemispherical, elastomeric surface using a robotic arm (UR3e, Universal Robots, Co). We used the robotic arm to record the force resulting from a displacement in either the x- or z-directions. We mounted the gripper as an end effector to the robotic arm and submerged it in a bath of water which completely covered the experimental surface. The experimental surface was a hemisphere composed of silicone rubber. To understand the effect of surface stiffness on the forces, we varied the surface from a stiff surface (stiffness, 0.165 MPa; Dragon Skin 10 Medium, Smooth-On, Inc.) to a soft surface (stiffness, 0.0065 MPa; Ecoflex 00-10, Smooth-On, Inc.). Prior to the measurements, a starting position was established, defined by the location where the suction disc began to contact the apex of the

hemispherical surface. To preload the disc slightly to the surface, we added an offset of 1 mm to the starting z-position. Trials began at the apex of the hemispherical surface.

During the shear measurements, the gripper translated in the x-direction for 30 mm at a rate of 0.5 mm $\cdot$ s^{-1}. During measurements of normal force, the gripper translated in the z-direction for 15 mm at a rate of 0.5 mm $\cdot$ s^{-1}. Each trial was run in triplicate and post-processed in MATLAB. We performed a linear interpolation on the data set from each trial, and averaged the interpolated force-displacement curves.

D. Applications of the gripper

The demonstration handling the marine sea cucumber was performed in an aquarium under the supervision of and permit to accredited Marine Biology Research Division Invertebrate Collector, P. Zerofski, from Scripps Institution of Oceanography.

ACKNOWLEDGMENT

We thank P. Zerofski for access to and supervision during the handling of sea cucumbers. Author Contributions: J.A.S., D.D.D., and M.T.T. conceived the project. J.A.S. designed and fabricated the gripper and experimental setups. T.X. performed the simulations of the actuator contacting a surface. I.A. and J.A.S. worked with the robotic arm to record force-displacement measurements of the gripper. J.A.S. performed manipulation demonstrations. J.A.S. prepared the initial draft of the manuscript and all authors provided feedback during revisions.

References

[1] K. Mizushima, T. Nishimura, Y. Suzuki, T. Tsuji, and T. Watanabe, "Surface texture of deformable robotic fingertips for a stable grasp under both dry and wet conditions," IEEE Robotics and Automation Letters, vol. 2, no. 4, pp. 2048–2055, 2017.

[2] M. S. Li, D. Melville, E. Chung, and H. S. Stuart, "Milliscale features increase friction of soft skin in lubricated contact," IEEE Robotics and Automation Letters, vol. 5, no. 3, pp. 4781–4787, 2020.

[3] H. Kinoshita, L. Backstrom, J. R. Flanagan, and R. S. Johansson, "Tangential torque effects on the control of grip forces when holding objects with a precision grip," Journal of Neurophysiology, vol. 78, no. 3, pp. 1619–1630, 1997.

[4] M. R. Cutkosky and P. K. Wright, "Friction, stability and the design of robotic fingers," International Journal of Robotics Research, vol. 5, no. 4, pp. 20–37, 1986.

[5] J. Shintake, V. Cacucciolo, D. Floreano, and H. Shea, "Soft robotic grippers," Advanced Materials, vol. 30, no. 29, p. 1707035, 2018.

[6] P. Glick, S. A. Suresh, D. Ruffatto, M. Cutkosky, M. T. Tolley, and A. Parness, "A soft robotic gripper with gecko-inspired adhesive," IEEE Robotics and Automation Letters, vol. 3, no. 2, pp. 903–910, 2018.

[7] P. Ditsche and A. P. Summers, "Aquatic versus terrestrial attachment: Water makes a difference," Beilstein Journal of Nanotechnology, vol. 5, pp. 2424–2439, 2014.

[8] H. S. Stuart, M. Bagheri, S. Wang, H. Barnard, A. L. Sheng, M. Jenkins, and M. R. Cutkosky, "Suction helps in a pinch: Improving underwater manipulation with gentle suction flow," IEEE/RSJ International Conference on Intelligent Robots and Systems, pp. 2279–2284, 2015.

[9] J. A. Sandoval, S. Jadhav, H. Quan, D. D. Deheyn, and M. T. Tolley, "Reversible adhesion to rough surfaces both in and out of water, inspired by the clingfish suction disc," Bioinspiration & Biomimetics, vol. 14, no. 6, p. 066016, 2019.

[10] T. Miyake, H. Ishihara, and M. Yoshimura, "Basic studies on wet adhesion system for wall climbing robots," IEEE/RSJ International Conference on Intelligent Robots and Systems, pp. 1920–1925, 2007.

[11] S. N. Gorb, "Biological attachment devices: exploring nature's diversity for biomimetics," Philosophical Transactions of the Royal Society A, vol. 366, pp. 1557–1574, 2008.

[12] Y. Chen, M.-C. Shih, M.-H. Wu, E.-C. Yang, and K.-J. Chi, "Underwater attachment using hairs: the functioning of spatula and sucker setae from male diving beetles," Journal of the Royal Society Interface, vol. 11, p. 20140273, 2014.

[13] J. K. Langowski, D. Dodou, M. Kamperman, and J. L. van Leeuwen, "Tree frog attachment: mechanisms, challenges, and perspectives," Frontiers in Zoology, vol. 15, p. 32, 2018.

[14] M. Varenberg and S. N. Gorb, "Hexagonal surface micropattern for dry and wet friction," Advanced Materials, vol. 21, pp. 483–486, 2009.

[15] J. A. Sandoval, J. Sommers, K. R. Peddireddy, R. M. Robertson-Anderson, M. T. Tolley, and D. D. Deheyn, "Toward bioinspired wet adhesives: Lessons from assessing surface structures of the suction disc of intertidal clingfish," ACS Applied Materials and Interfaces, vol. 12, no. 40, pp. 45460–45475, 2020.

[16] M. Varenberg and S. Gorb, "A beetle-inspired solution for underwater adhesion," Journal of the Royal Society Interface, vol. 5, no. 20, pp. 383—385, 2008.

[17] Y. Wang, V. Kang, E. Arzt, W. Federle, and R. Hensel, "Strong wet and dry adhesion by cupped microstructures," ACS Applied Materials and Interfaces, vol. 11, no. 29, pp. 26483–26490, 2019.

[18] H. Chen, L. Zhang, D. Zhang, P. Zhang, and Z. Han, "Bioinspired surface for surgical graspers based on the strong wet friction of tree frog toe pads," ACS Applied Matierals and Interfaces, vol. 7, no. 25, pp. 13987–13995, 2015.

[19] F. Meng, Q. Liu, X. Wang, D. Tan, L. Xue, and W. J. P. Barnes, "Tree frog adhesion biomimetics: Opportunities for the development of new, smart adhesives that adhere under wet conditions," Philosophical Transactions of the Royal Society A, vol. 377, no. 2150, p. 20190131, 2019.

[20] P. V. Nguyen and V. A. Ho, "Mechanics of wet adhesion in soft interaction with patterned morphology," Bioinspiration & Biomimetics, vol. 14, no. 1, p. 016005, 2019.

[21] P. Polygerinos, N. Correll, S. A. Morin, B. Mosadegh, C. D. Onal, K. Petersen, M. Cianchetti, M. T. Tolley, and R. F. Shepherd, "Soft robotics: review of fluid-driven intrinsically soft devices; manufacturing, sensing, control, and applications in human-robot interaction," Advanced Engineering Materials, vol. 19, no. 12, p. 1700016, 2017.

[22] P. V. Nguyen, Q. K. Luu, Y. Takamura, and V. A. Ho, "Wet adhesion of micro-patterned interfaces for stable grasping of deformable objects," IEEE International Conference on Intelligent Robots and Systems, pp. 9213–9219, 2020.

[23] M. Cianchetti, C. Laschi, A. Menciassi, and P. Dario, "Biomedical applications of soft robotics," Nature Reviews Materials, vol. 3, no. 6, pp. 143–153, 2018.